Since January 2020 Elsevier has created a COVID-19 resource centre with free information in English and Mandarin on the novel coronavirus COVID-19. The COVID-19 resource centre is hosted on Elsevier Connect, the company's public news and information website.

Antimicrobial Coatings Based on Linseed Oil/TiO_2 Nanocomposites

19

Ana M. Díez-Pascual
Alcalá University, Madrid, Spain

1. Introduction

Worldwide demand for bio-based products derived from renewable biomass has augmented spectacularly over the last few years due to the global environmental concern and the sharp rise in petroleum price. In this context, cost-effective, sustainable, and eco-friendly polymeric materials derived from renewable resources that can replace those based on petroleum feedstock are being sought. Even after the recent expansion of renewable polymers, the small contribution of renewable polymers in the commercial market is mostly due to their elevated cost and poorer performance compared with synthetic polymers produced from petroleum chemicals [1]. The leading challenge for the biorenewable industry is to prepare materials with properties that counterpart those of petroleum-based ones so that they can compete or even surpass the chemicals now in use. The most-employed renewable resources are plant oils, polysaccharides, and proteins.

Vegetable or plant oils constitute a renewable resource that can be used as starting material for polymers due to their abundant availability, relatively low cost, biodegradability, and environmental friendship [2]. The major constituents of plant oils are triglycerides, which are the product of esterification of glycerol with three fatty acids. Fatty acids account for 95% of the total weight of triglycerides, and their composition varies depending on the plant, crop, season, growing conditions, and purification methods [3], and their properties are conditioned by the stereochemistry of the double bonds, the degree of unsaturation and the length of fatty acids. The chemical structures of the most common fatty acids of vegetable oils are depicted in Fig. 19.1.

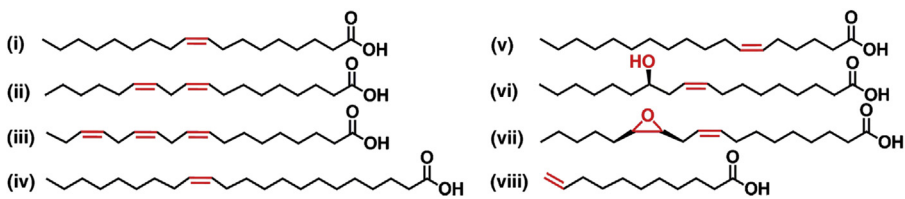

Figure 19.1 Most common fatty acids of vegetable oils include: (i) oleic acid, (ii) linoleic acid, (iii) linolenic acid, (iv) erucic acid, (v) petroselinic acid, (vi) ricinoleic acid, (vii) vernolic acid, (viii) 10-undecenoic acid.

Handbook of Antimicrobial Coatings. http://dx.doi.org/10.1016/B978-0-12-811982-2.00019-6

Linseed, sunflower, castor, soybean, oiticica, palm, tall, olive, cottonseed, jatropha, and rapeseed oils are most commonly used for the synthesis of biopolymers [4,5] and have found practical applications as biodiesel, lubricants, cutting fluids, coatings surfactants, soaps, cosmetic products, and so forth. A number of derivatives of vegetable oils have been employed as polymerizable monomers in radiation-curable systems to provide flexible and tough resins like epoxy, urethane, and polyester [6]. Amine-cured combinations of epoxidized soybean oil and conventional epoxy resins, acrylated soybean oil copolymerized with styrene and divinylbenzene, and polyurethane resins prepared from polyols derived from castor oil have been widely used to prepare composite materials with excellent mechanical and barrier properties [7]. Further, epoxidized vegetable oils (EVO) such as soybean and palm have been used in UV-curable coating systems [5,6]. While the use of vegetable oils in paints and coatings is decades old, nowadays emphasis is being made on this type of materials to bring in new properties, improved performance coupled with environment friendliness at affordable costs [8]. It is expected that vegetable oil—based coating will compete in the next future with their petro-based counterparts in performance and applications and may establish themselves as "greener" precursors to environment friendly coatings.

Linseed oil (LO), also known as flaxseed oil or flax oil, is a colorless to yellowish oil obtained from the dried, ripened seeds of the flax plant (*Linum usitatissimum* L.), widely cultivated in Europe for selected industrial applications, specifically oils and fibers [9]. This oil is beneficial for the human body and can prevent heart attack since it is the richest source of α-linolenic acid. It also contains lignans that may have antioxidant actions and aid to protect against certain cancers. In addition, it helps to prevent elevated blood pressure by inhibiting inflammatory reactions that cause artery-hardening plaque and poor circulation. About 70% of all the LO produced worldwide is intended for technical applications, and the rest is for food production. Its typical fatty acid composition is shown in Fig. 19.2. The low cost, sustainability, availability, and ease of handling of LO make it attractive as an alternative to petroleum-based plastics. Consequently, it has previously been employed as raw material for the synthesis of biopolymers [10] as well as in paints and coatings, and it is starting to be used in agriculture, food packaging, and biomedicine. In this regard, the antibacterial activity of LO against *Escherichia coli*, *Staphylococcus aureus, Enterococcus faecalis*, *Micrococcus luteus,* and *Candida albicans* has been recently reported [11].

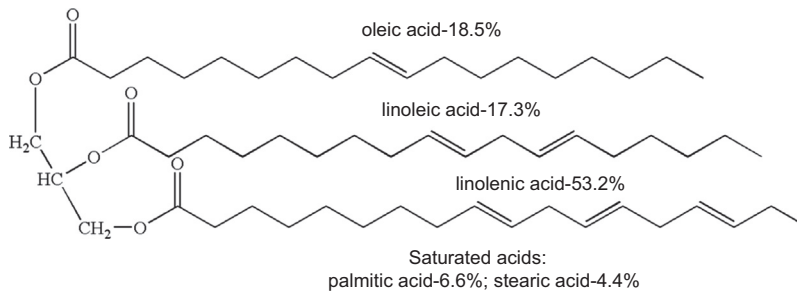

Figure 19.2 Fatty acid composition for linseed oil.

Polymers derived from vegetable oils exhibit poor mechanical and barrier properties, which limit their practical applications [1]. In particular, their brittleness, high gas and vapor permeability, low heat distortion temperature, and poor resistance to prolonged processing operations have restricted their industrial uses. To overcome these shortcomings, with a view to expand their range of commercial uses, new approaches are required such as blending with other polymers [12] or filling with nanofillers [13−16]. The incorporation of nanofillers into EVO-based thermosetting polymers results in bionanocomposites with enhanced performance [13,14].

Titanium dioxide (TiO_2) is a semiconductor material appropriate for a broad range of applications, including photocatalysis, environmental pollution control, and solar energy conversion owing to its strong oxidizing power, nontoxicity, low cost, strong UV absorption, and high antibacterial activity versus a great selection of microorganisms, including algae, viruses, fungi, and bacteria [17]. One of the leading applications of photocatalytic coatings, including TiO_2 particles, is to avoid microbial growth or, at least, decrease the amount of microorganisms that proliferate on indoor building materials [18]. Indoor air pollution is a severe public health concern and a major reason for mortality worldwide. The presence of microbial populations in humid indoor environments is one of the main causes of the sick building syndrome [19]. Further, a direct correlation between mold growth and respiratory diseases for people who occupy damp or water-damaged buildings has been found [20]. Microorganisms can produce contaminants like allergens or toxins that cause health problems to occupants such as allergic reactions, respiratory infections, asthma, pneumonitis, chronic rhinosinusitis, and so forth.

Up to date, a great number of articles dealing with biopolymer/TiO_2 composites suitable for different applications have been published [21−24]. Nonetheless, works on photocatalytic and/or antimicrobial coatings based on TiO_2-reinforced biopolymers are very scarce [25−27]. Thus, the photocatalytic activity of aliphatic polyester/TiO2 biodegradable films prepared by blown film extrusion [25], the self-cleaning properties of polycaprolactone/TiO_2 nanocomposites synthesized via solution-casting method [26], and the anticorrosive and antimicrobial properties of castor oil−based poly(urethane-ester amide)/TiO_2 coatings have been reported [27].

The present chapter focuses on the preparation and characterization of novel acrylated epoxidized linseed oil (AELO)-based bionanocomposites reinforced with anatase TiO_2 nanoparticles with a view to use them as antimicrobial coatings. AELO was synthesized from the EVO using acrylic acid as ring opening agent, triethylamine (TEA) as a catalyst, and hydroquinone as a free radical inhibitor, subsequently cross-linked and subjected to UV irradiation to get the cured nanocomposites. Their morphology, barrier, thermal, mechanical, tribological, and antibacterial properties have been analyzed through a variety of techniques. The following sections will describe in detail the influence of the nanoparticle concentration on the different properties. These antimicrobial nanocomposites are suitable for the surface coating industry. Thus, they can be applied to frequently touched objects in public places such as hospitals, schools, restaurants, public transportation, etc. More importantly, they can be appropriate as coatings for hospital countertops, beds, and general medical tools, and in particular, in operating rooms where it is easier to acquire a contagion.

Even though decontamination and disinfection of surfaces using chemicals is a frequent practice to avoid spread of diseases, such protocols are sometimes skipped or not practicable. Therefore, these nanocomposite coatings could be very useful to prevent bacterial infection in public places.

2. Titanium Dioxide: Structure, Synthesis, Properties, and Applications

2.1 Structure

TiO_2 is a transition metal oxide that exists in four mineral forms [28]: anatase (tetragonal), brookite (orthorhombic), rutile (tetragonal), and TiO_2 (B) (monoclinic). In addition, two high-pressure forms, TiO_2 (II) with a PbO_2 structure and TiO_2 (H) with a hollandite structure have been synthesized from the rutile phase. Anatase TiO_2 has a tetragonal structure (Fig. 19.3A) and encloses six atoms per unit cell, albeit the TiO_6 octahedron is distorted. The anatase phase predominates at 0 K; this structure is ideal for solar cell applications due to higher electron mobility, higher specific area, lower dielectric constant, and density. Rutile TiO_2 also has a tetragonal structure (Fig. 19.3B) and the octahedron is less distorted. It is stable at most temperatures and pressures up to 60 kbar. Anatase and brookite structures transform to the rutile phase for particle sizes >14 nm. It is mainly used as white pigment in paint. Brookite TiO_2 belongs to the orthorhombic crystal system (Fig. 19.3C). Its unit cell comprises eight formula units of TiO_2 and is formed by edge-sharing TiO_6 octahedra.

2.2 Synthesis

TiO_2 can be synthesized with different morphologies like nanotubes, nanowires, nanorods, and mesoporous structures. A variety of synthesis methods such as hydrothermal, solvothermal, sol−gel, direct oxidation, chemical vapor deposition (CVD), electrodeposition, sonochemical, mechanochemical, and microwave method have been used for the preparation of TiO_2 nanostructures [29]. Among them, the most employed are the sol−gel and the hydrothermal method. The former process involves conversion of monomers into a colloidal solution (*sol*) that acts as the precursor for the discrete

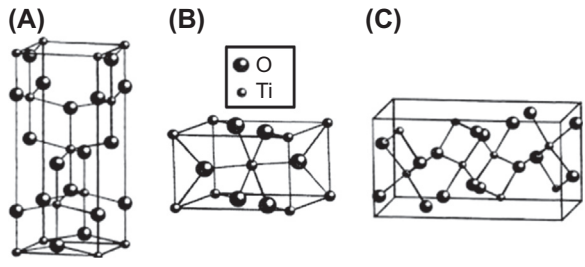

Figure 19.3 Crystal structure of titanium dioxide (TiO_2): (A) anatase; (B) rutile; (C) brookite.

particles. This process normally proceeds via an acid-catalyzed hydrolysis step of titanium (IV) alkoxide followed by condensation. The latter does not necessitate the use of organic solvents or further processing of the product (grinding and calcination), which makes it a straightforward and environmentally friendly technique. The synthesis occurs in an autoclave, where the mixture of substrates is heated steadily to a temperature of 100−300°C and is kept for several days. This process leads to products of high degree of crystallinity and high purity. The mechanochemical process is an inexpensive and easy method of obtaining TiO_2 nanoparticles on a large scale [30]. It employs titanyl sulfate ($TiOSO_4 \cdot xH_2SO_4 \cdot yH_2O$) as starting material and requires high-energy dry milling that starts a reaction through ball−powder impact in a ball mill at low temperature. A "thinner" is added to the system in the form of a solid (usually NaCl), which acts as a reaction medium and separates the nanoparticles being formed. The advantages of this technique are the high homogeneity of the crystalline structure and morphology, low production costs, small particle sizes, and restricted tendency of the particles to agglomerate. A shortcoming of this method is that it requires long milling times to attain a uniform grinding of the powder, which leads to a greater amount of impurities.

In the sonochemical method, a solution of the precursor (typically tetraisopropyl titanate) in NaOH is exposed to ultrasound for several minutes (c. 30) under ambient conditions. The resulting precipitates are then centrifuged, washed with deionized water several times, and finally dried [31]. In the microwave heating, the solution is heated using microwaves at 90°C for a few minutes. The precipitate obtained is then centrifuged, washed with water and ethanol, and finally dried. These methods of obtaining TiO_2 enable high yields, in excess of 90%, do not require surfactants, can be applied on a large scale with low production costs, and are simple and energy efficient.

Electrodeposition is frequently employed to make a coating on a surface by the reduction at the cathode. The substrate to be coated is used as cathode and immersed into a solution that contains a salt of the metal to be deposited. TiO_2 nanowires can be obtained by electrodeposition using a template of an anodic alumina membrane [32]. Typically, the electrodeposition is performed in 0.2 M $TiCl_3$ solution at pH = 2, and titanium is deposited into the pores of the membrane, followed by heating at 500°C for 4 h. CVD processes are also used to fabricate coatings. They usually take place within a vacuum chamber: thermal energy heats the gases in the coating chamber and drives the deposition reaction. Crystalline TiO_2 films with grain sizes below 30 nm and TiO_2 nanoparticles <10 nm can be prepared by pyrolysis of titanium tetraisopropoxide in a mixed helium/oxygen atmosphere.

2.3 Properties

Recently, titania (TiO_2) nanostructures have involved much interest within the scientific community as "future materials" due to their low cost, stability, easy availability, possibility of performing surface modifications with different functional groups, and biocompatibility. They are semiconductors with a structurally dependent band gap (anatase—3.20 eV and rutile—3.03 eV), widely used for optoelectronic and

photocatalytic applications. In particular, they are very effective in photocatalytic water splitting and have been employed as active layers in photovoltaics as well as electrodes in photoelectrolysis cells where they have been shown to enhance the efficiency of electrolytic splitting of water into hydrogen and oxygen [33]. These environmentally friendly materials also display intense UV absorption, large volume to area ratio, high catalytic activity, highly crystalline structure, radiation hardness, density of ~ 4 g/cm^3, melting point of 2100 K, good mechanical properties including a Young's modulus of 230 GPa and hardness of ~ 10 GPa, low coefficient of thermal expansion ($\sim 8.4 \times 10^{-6}$ K^{-1} at 300 K), low dielectric constant (~ 10), and high thermal conductivity (~ 4.8 W/cm K). They also display antimicrobial activity against a large variety of microorganisms, including algae, viruses, protozoa, fungi, and bacteria like *Saccharomyces cerevisiae* (yeast), *Lactobacillus acidophilus* and *E. coli* (bacteria), and *Chlorella vulgaris* (green algae). When TiO_2 is illuminated with UV light, electron (e−)/hole (h+) pairs are generated that have strong reducing and oxidizing power. These react with O_2 and H_2O to form reactive oxygen species (ROS) including superoxide anion radicals (O^{2-}) and hydroxyl radicals (•OH) (Fig. 19.4), which are regarded the dominant species contributing to the destruction of microorganism cells [34]. The hydroxyl radical is an extremely aggressive oxidant, and as such, it can attack various biological molecules and impair their proper functioning.

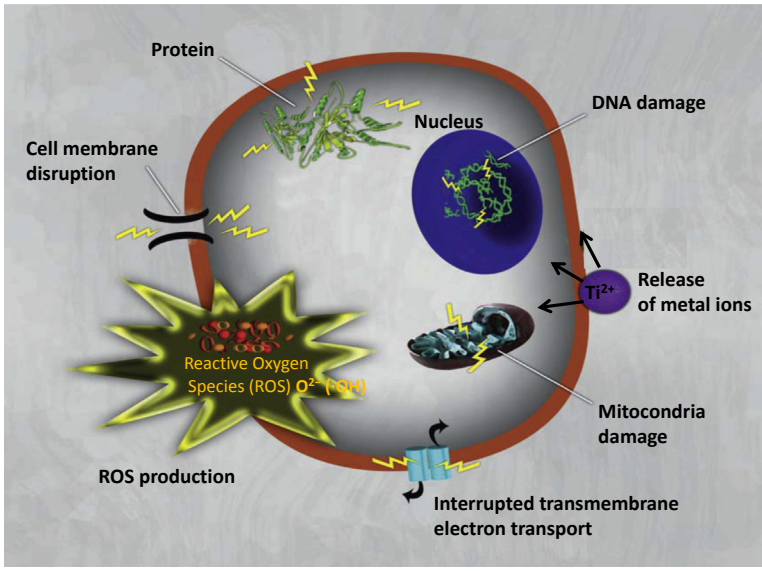

Figure 19.4 Mechanisms of antibacterial activity of nanoparticles against bacteria. Adapted from M.J. Hajipour, K.M. Fromm, A.A. Ashkarran, D. Jimenez de Aberasturi, I. Ruiz de Larramendi, T. Rojo, V. Serpooshan, W.J. Parak, M. Mahmoudi, Antibacterial properties of nanoparticles, Trends Biotechnol. 30 (2012) 499−511, copyright 2012, with permission from Elsevier.

Other mechanisms of antibacterial activity have been proposed, including membrane disorganization due to accumulation of TiO_2 nanoparticles in the bacterial membrane and also their cellular internalization (Fig. 19.4); bacterial death seems to be caused by a disorder in the cell permeability and decomposition of the cell walls. It has been reported that cell wall damage precedes cytoplasmic membrane damage [36], thereby leading to leakage of minerals, proteins, and genetic materials, causing cell death. For instance, cell membrane damage took place due to the photocatalytic degradation of endotoxin from *E. coli* with TiO_2 thin films [36]. Further, it has been demonstrated that the rate of adsorption of cells onto TiO_2 is directly related to its bactericidal effect [37]. Adsorption of cells onto aggregated TiO_2, followed by loss of membrane integrity, was the reason of the bactericidal effect. Another explanation of the antimicrobial action is the release of Ti^{2+} ions that bind to the membrane of the microorganisms.

2.4 Applications

The applications of TiO_2 nanomaterials comprise paint, toothpaste, UV protection, photocatalysis, photovoltaics, sensing, electrochromics, and photochromics. Their optical and biocompatible properties make them suitable for UV-blocking applications. They act as antifogging agents and prevent the condensation of water in the form of small droplets on glass products like mirrors and eyeglasses. They have also been used as sensors for gases and humidity due to the change in electrical or optical properties on adsorption [38], and for water splitting and hydrogen production due to their electronic band structure [39]. They can be used for the photocatalytic decomposition of various pollutants, in solar cell applications, and to make photochromic devices in combination with dyes [40].

3. Preparation of AELO/Titanium Dioxide Nanocomposite Coatings

3.1 Synthesis of Epoxidized Linseed Oil

The synthesis procedure of epoxidized linseed oil (ELO) is depicted in Fig. 19.5. The epoxidation was performed in a four-necked glass flask equipped with a mechanical stirrer, thermometer, and reflux condenser. Firstly, LO ($d_{25°C} = 0.93$ g/cm^3, $M_w \sim 890$ g/mol; iodine number = 177; oxidation level = 0.95; acid value = 0.8; saponification value = 190) and formic acid were mixed for 10 min at 55°C [41]. H_2O_2 was then added dropwise to the mixture for 1 h; 1:1.8 C═C:H_2O_2 mole ratios were used, and the reaction was allowed to continue for 4 h. The mixture was cooled down and the product was filtered, washed with water repeatedly until pH = 7.0, and dried in an oven at 60°C for 12 h. The oxirane content was determined as 8.9% via titration of the epoxy groups with hydrobromic acid solution [41].

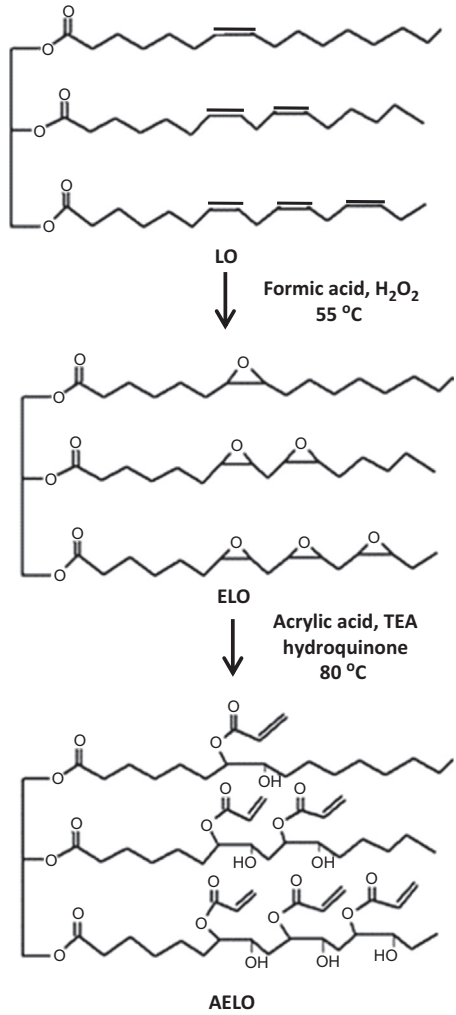

Figure 19.5 Synthesis procedure of epoxidized linseed oil (ELO) and acrylated epoxidized linseed oil (AELO).
Reprinted from A.M. Diez-Pascual, A.L. Diez-Vicente, Development of linseed oil−TiO_2 green nanocomposites as antimicrobial coatings, J. Mater. Chem. B 3 (2015) 4458−4471, copyright 2015, with permission from the Royal Society of Chemistry.

3.2 Acrylation of Epoxidized Linseed Oil

AELO was synthesized from ELO by means of ring opening of the epoxy group with acrylic acid using TEA as a catalyst and hydroquinone as a free radical inhibitor (Fig. 19.5). A mixture of ELO and acrylic acid (6:1 w/w) in the presence of TEA was heated up to 110°C under continuous stirring. The reaction continued for 30 h until a constant acid value of ∼8 mg KOH/g was attained. Unreacted acrylic acid

and TEA were eliminated via petroleum ether/water extraction. The degree of esterification, calculated from the acid value at the beginning and end of the reaction, was 88% [41].

3.3 Preparation of the UV-Curable Nanocomposites

The nanocomposites were prepared via UV curing using the AELO resin (65%−70%), trimethylolpropane trimethacrylate (TMPTMA) as the cross-linking monomer (23%−25%), benzophenone (BP) as the photoinitiator (3.5%−3.2%) along with 2-dimethylaminoethanol (DMAE) as a catalyst (1.5%), and TiO_2 nanopowder (99.8% anatase, $d_{25°C} = 4.26$ g/cm^3, <100 nm particle size, and specific surface area >14 m^2/g) as nanofiller. Four nanocomposites were prepared, with TiO_2 loading of 1.0, 2.5, 5.0, and 7.5 wt%. The mixtures were finally coated on glass plates and cured under UV light, leading to coatings about 140−160 μm thick.

4. Characterization of the Nanocomposite Coatings

4.1 Morphology and Structure

The surface morphology of AELO/TiO_2 coatings was analyzed by scanning electron microscopy coupled to an energy dispersive X-ray detector (EDAX). As depicted in Fig. 19.6A for AELO/TiO_2 (7.5 wt%) nanocomposite, the coatings are uniform without detectable cracks. Brilliant spherical dots well dispersed inside the AELO matrix can be observed, which correspond to the TiO_2 nanoparticles that have an average diameter of 40 nm. They are mostly individually dispersed, albeit some small clusters comprising a few nanoparticles are also found. Similar morphology was found for the rest of nanocomposites [41]. The H-bonding and polar interactions between the OH groups of TiO_2 surface and the polar groups of AELO prevent the formation of nanoparticle aggregates. Hence, good dispersion of TiO_2 was achieved without the need for particle surface treatments or compatibilizing agents, which makes the fabrication of these nanocomposites easier, cheaper, and more environmentally friendly. The EDAX spectrum of the nanocomposite (Fig. 19.6B) corroborates that the sample contains Ti, C, N, and O elements, thus confirming the presence of the nanoparticles entrapped within the epoxidized network.

Their structure was analyzed by X-ray diffraction recorded using a Cu tube as X-ray source (λ CuK$\alpha = 1.54$ Å), and the diffractogram of AELO/TiO_2 (7.5 wt%) nanocomposite is shown in Fig. 19.6C. AELO exhibits a single wide reflection at ~17 degrees indicating its amorphous nature. TiO_2 nanoparticles show peaks at 2θ values of 25.2, 38.3, 39.2, 48.3, 54.4, and 55.6 degrees corresponding to the diffraction of the (101), (004), (112), (200), (105), and (211) planes, respectively, of the tetragonal structure of anatase TiO_2 [24]. These peaks are also observed in the nanocomposites, which corroborates that the crystalline structure of the nanoparticles is maintained after the UV-curing process, albeit the peaks are wider and slightly shifted upward compared with those of the raw nanoparticles, suggesting a change in the unit cell dimensions.

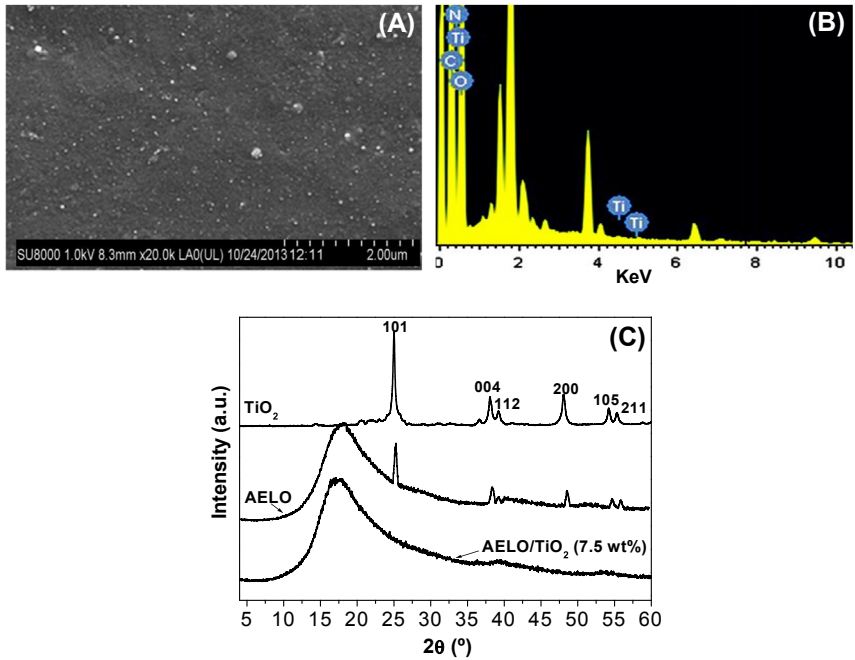

Figure 19.6 (A) Scanning electron microscopy micrograph and (B) energy dispersive X-ray detector of cured acrylated epoxidized linseed oil (AELO)/titanium dioxide (TiO_2) (7.5 wt%) nanocomposite coating. (C) X-ray diffraction pattern of TiO_2 nanoparticles, cured AELO, and AELO/TiO_2 (7.5 wt%) nanocomposite.
Adapted from A.M. Diez-Pascual, A.L. Diez-Vicente, Development of linseed oil−TiO_2 green nanocomposites as antimicrobial coatings, J. Mater. Chem. B 3 (2015) 4458−4471, copyright 2015, with permission from the Royal Society of Chemistry.

Further, the nanocomposite presents smaller crystallite size, attributed to the steric effect of the nanoparticles neighboring to the AELO chains that hinder their molecular packing, resulting in smaller crystals.

4.2 Thermal Properties

The thermal stability of the UV-cured coatings was investigated by thermogravimetric analysis (TGA) under a nitrogen atmosphere [41]. The coatings were dried overnight at 80°C and then heated from 100 to 550°C, and the thermograms are shown in Fig. 19.7A. TiO_2 nanoparticles exhibit two small degradation stages, one below 300°C ascribed to the elimination of surface adsorbed water and the other related to the removal of residual organic material at ~340°C. AELO is thermally stable up to ~300°C, and exhibits two decomposition steps too; the first attributed to the loss of functional groups and the second to the degradation of the epoxy chains. Similar thermogram is found for the nanocomposites, suggesting that the degradation

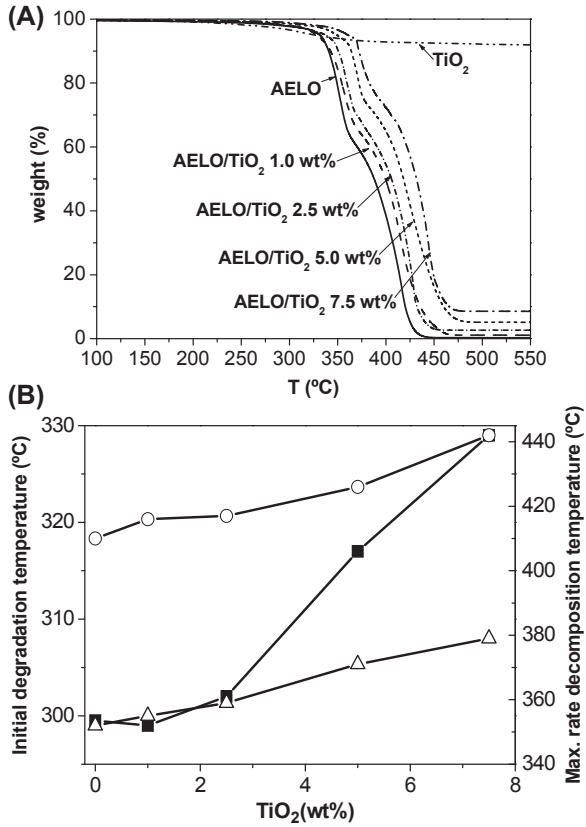

Figure 19.7 (A) Thermogravimetric analysis curves under nitrogen atmosphere for acrylated epoxidized linseed oil (AELO)/titanium dioxide (TiO_2) nanocomposites. (B) Initial degradation temperature (*solid squares*) and maximum rate decomposition temperature (the open *triangles and circles* correspond to the first and second degradation stage, T_{max1} and T_{max2}, respectively).

mechanism of AELO remains unchanged in the presence of TiO_2, although the curves are upshifted. As can be observed in Fig. 19.7B, the initial degradation temperature (measured at 2% weight loss) and the temperatures of maximum rate decomposition (T_{max1} and T_{max2} referring to the first and second degradation stages) increase with increasing TiO_2 content, by up to 30, 27, and 34°C, respectively, for the AELO/TiO_2 (7.5 wt%) nanocomposite. This behavior is ascribed to the high thermal conductivity of TiO_2 that allows a more rapid heat dissipation within the nanocomposite and the barrier effect of the nanoparticles that hinder the diffusion of decomposition products.

To improve flammability, it is beneficial if nanocomposites enhance char formation during combustion [42]. TGA curves show an increase in char residue with increasing TiO_2 loading, from 0.4% for AELO to 9% for the nanocomposite with 7.5 wt% nanoparticle content, indicating improved flame resistance of the coatings, which is likely

connected to the barrier effect of the nanoparticles that form a tortuous path that can delay the diffusion of the gas molecules through the polymer, and to the high aspect ratio of the nanoparticles that leads to a big TiO_2/AELO interfacial contact area, facts that are intensified with increasing nanoparticle loading.

4.3 Barrier Performance

The permeability of coatings to water and oxygen are key parameters influencing their corrosion stability. Consequently, low moisture absorption and low oxygen permeability are highly desired. The water uptake, water vapor permeability (WVP), and oxygen permeability of AELO/TiO_2 nanocomposite coatings were measured, and the results are shown in Fig. 19.8. To determine the water uptake, the coatings were first dried in a desiccator at 0% RH for 1 week and then placed in a beaker at 100% RH and allowed to absorb water at 25°C. Water absorption was calculated as: $[(W_f - W_i)/W_i] \times 100$, where W_i and W_f are the initial (dried) and final (wet) weight of the nanocomposites, respectively.

The water uptake of AELO (about 4%) is related to the free volume and the acrylic ester groups of the polymeric chains that tend to absorb water by hydrolysis. The water uptake decreases strongly with increasing nanoparticle loading, by up to 33% for the nanocomposite with 7.5 wt% TiO_2, due to the increase in H-bonding that reduces the free water molecules [41] and the increased tortuosity of the transport pathway for water molecules. Analogous behavior was reported for epoxidized soybean oil/montmorillonite nanocomposites [43], where the water uptake decreased with increasing nanoclay concentration due to a stronger tortuosity effect.

WVP was measured at 25°C using Payne permeability cups. WVP was calculated as: $WVP = (\Delta m \times l)/(A \times t \times \Delta P)$, where Δm is the weight loss of each cup, l the thickness of the film, A the contact area, t the time, and ΔP the partial pressure

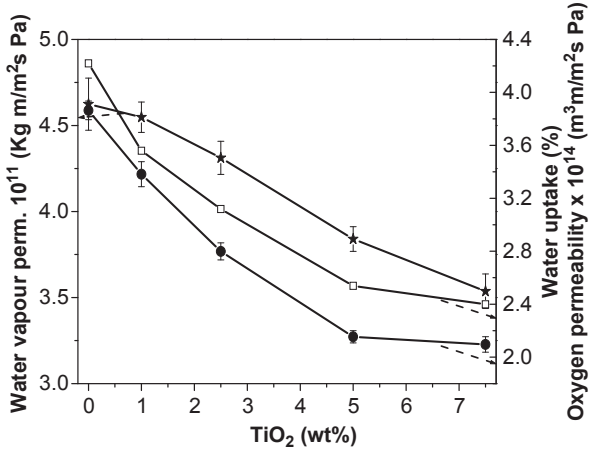

Figure 19.8 Water uptake (*open squares*), water vapor permeability (*solid stars*), and oxygen permeability (*solid circles*) of AELO/TiO_2 nanocomposites.

difference between inside and outside of the cup. Oxygen permeability was evaluated by measuring the oxygen transference rate (OTR) with a gas permeability tester and calculated as: $(OTR \times l)/\Delta P$. As can be observed in Fig. 19.8, both properties also decrease with increasing TiO_2 loading, leading to 21% and 45% reductions compared with AELO, respectively, at the highest nanoparticle content. These results indicate superior barrier properties to gases for the nanocomposite coatings compared to neat AELO. Previous studies have also reported reduced WVP in epoxy/TiO_2 nanocomposites [44]. Other researchers have also shown positive effects of TiO_2 nanoparticles on WVP of epoxy-based nanocomposites [31]. The drop in oxygen permeability is considerably stronger than that in water uptake, attributed to the different size and polarity of water and oxygen molecules. Thus, the former molecules are smaller, hence can penetrate the coatings more easily, leading to a smaller reduction.

4.4 Mechanical Properties

Dynamic mechanical properties were studied using a dynamic mechanical analyzer at a frequency of 1 Hz. The storage modulus E' and tan δ (ratio of the loss to storage modulus) were recorded as a function of temperature, as shown in Fig. 19.9. E' of

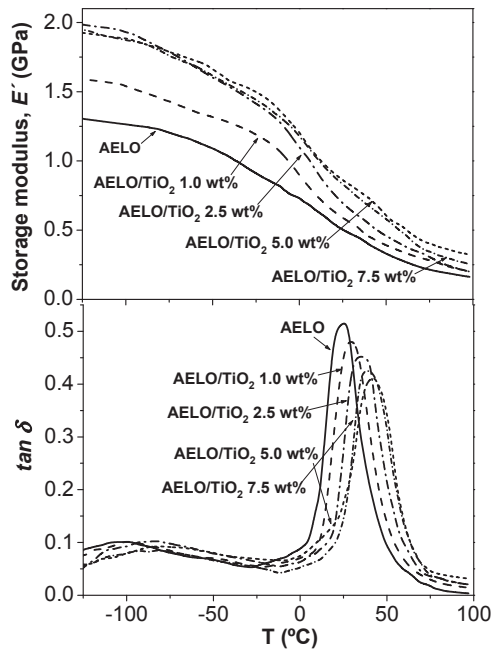

Figure 19.9 Storage modulus E' and tan δ of acrylated epoxidized linseed oil (AELO)/titanium dioxide (TiO_2) nanocomposite coatings as a function of temperature.
Adapted from A.M. Diez-Pascual, A.L. Diez-Vicente, Development of linseed oil−TiO_2 green nanocomposites as antimicrobial coatings, J. Mater. Chem. B 3 (2015) 4458−4471, copyright 2015, with permission from the Royal Society of Chemistry.

the nanocomposite coatings increases with increasing nanoparticle loading, indicating that the mechanical load is effectively transferred from the matrix to the nanoparticles. A maximum increase of 80% is found for the nanocomposite with 5.0 wt% TiO_2 compared to AELO with 20°C. Nonetheless, higher nanoparticle loadings do not result in improved modulus, likely due to the presence of small particle clusters.

Tan δ versus temperature curves exhibit two relaxation peaks: one at low temperature (β-transition) ascribed to the movement of [$-CH_2-CH(OH)-CH_2-$] aliphatic segments, and other at higher temperature (α-transition) ascribed to Brownian motion of the polymeric chains at the transition from the glassy to the rubbery state (glass transition temperature, T_g). The addition of TiO_2 shifts the curves toward higher temperatures: T_g increases by up to 17°C for the nanocomposite with 5.0 wt% TiO_2 compared with AELO, ascribed to strong matrix−nanofiller interactions that limit the motion of the polymer chains. Nonetheless, higher TiO_2 contents lead to a small decrease in T_g due to the presence of small particle aggregates. Further, a broadening of tan δ peak is found for the nanocomposites, ascribed to the heterogeneous nature of the nanocomposites given that the polymer chains nearby the nanoparticles differ from those located in the bulk. The area under tan δ peak is greater for the nanocomposites, indicating better capability to absorb energy during deformation, hence higher impact resistance.

Indentation tests were performed via instrumented indentation technique at 23°C and 40% RH on the cross-sectional surface of the coatings using a CSM Micro-Hardness Tester with a Berkovich indenter [45]. In each run, the indenter was driven into the coating surface at a rate of 0.15 mN/s until a peak load of 4.0 mN was attained and held for 5 s to minimize the effect of viscoelastic deformation, and then unloaded at the same rate. The indentation hardness (H) value was defined as:

$$H = \frac{P_{\max}}{A_c} \tag{19.1}$$

where $P_{\max}$ is the maximum applied load measured at the maximum depth of penetration ($h_{\max}$) and A_c is the projected contact area at that load. The reduced modulus E_r can be calculated from the contact stiffness S, dP/dh, and A_c as follows:

$$E_r = \frac{\sqrt{\pi}}{2\beta}\frac{S}{\sqrt{A_c}} \tag{19.2}$$

where

$$\frac{1}{E_r} = \frac{\left(1-\nu^2\right)}{E}\frac{\left(1-\nu_i^2\right)}{E_i} \tag{19.3}$$

where β is 1.034 for a Berkovich indenter, E and ν are the elastic modulus and Poisson's ratio of the material, respectively, and E_i and ν_i are 1141 GPa and 0.07 (for a diamond indenter).

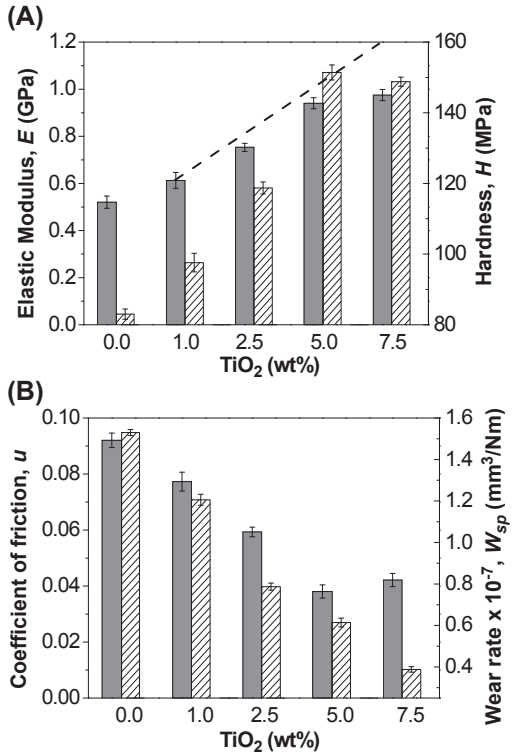

Figure 19.10 (A) Elastic modulus (*solid bars*) and hardness (*dashed bars*); (B) coefficient of friction (*solid bars*) and wear rate (*dashed bars*) as a function of titanium dioxide (TiO_2) content. The *dashed line* in (A) shows the predictions by the Krenchel's rule of mixtures.

The mean hardness (*H*) and elastic modulus (*E*) values obtained from the indentation tests versus TiO_2 content are shown in Fig. 19.10A. AELO has an *E* value of ~0.5 GPa, which increases on increasing TiO_2 concentration, by up to 94% for the nanocomposite with 7.5 wt% loading, attributed to the reinforcement effect of the well-dispersed stiff nanoparticles along with the strong matrix−nanoparticle H-bonding interactions that favor an effective load transfer.

The elastic modulus of filler-reinforced composites can be estimated by the Krenchel's rule of mixtures [46]:

$$E = (\eta E_f - E_m)V_f + E_m \tag{19.4}$$

where E_f and E_m are the filler and matrix modulus, respectively, V_f the volume fraction of the filler, and η a coefficient that is supposed to be 0.2 for randomly oriented fillers. Taking into account the high modulus of TiO_2 (230 GPa), the theoretical *E* values of the nanocomposite coatings were calculated using Eq. (19.4), and are plotted as a dashed line in Fig. 19.10A.

The theoretical values are in very good agreement with the experimental data up to TiO_2 contents of 5.0 wt%. Since the model presumes nanoparticles individually dispersed within the matrix and ideal nanofiller−matrix adhesion, this confirms that at low loadings the nanoparticles are definitely homogeneously dispersed and strongly adhered to AELO. Nevertheless, the experimental data of the nanocomposite with 7.5 wt% TiO_2 is nearly 20% lower than the theoretical value, ascribed to the presence of small agglomerates that have a negative effect on the mechanical performance.

The hardness also rises with increasing TiO_2 loading, by up to 73% at 5.0 wt%, ascribed to the hardening effect of the homogeneously dispersed nanoparticles. As the TiO_2 concentration increases, the interparticle distance diminishes, whereas the matrix−nanoparticle interactions turn out to be stronger, thus the hardening is more prominent. On the other hand, a small drop in this property is found for the nanocomposite with 7.5 wt% loading, suggesting less potential to hold up the applied load imposed by the indenter. At such loading, the nanoparticles are less uniformly distributed within the AELO resin, thus the free volume might increase, favoring the motion of the polymeric segments, and as a consequence, H falls to some extent.

4.5 Tribological Properties

Coatings are commonly employed to decrease friction and protect the substrate surface from wear. It has been reported that vegetable oils can create lubricant films that interact strongly with metallic surfaces, diminishing both friction and wear [47]. The characteristics of a lubricating coating are influenced by its forces of interaction with the substrate; weak interfacial adhesion results in coating delamination, and the existence of pores worsens the barrier performance and consequently the tribological properties. In this regard, the tribological performance of the nanocomposite coatings was evaluated at room temperature with a pin-on-disc tribometer under a load of 1 N, with a 6-mm diameter 100Cr6 steel ball as counterpart [41]. The results for the coefficient of friction (μ) and the specific wear rate (W_{sp}) of the nanocomposite coatings are plotted in Fig. 19.10B. μ decreases gradually with TiO_2 content, by about 57%, for the nanocomposite with 5.0 wt% concentration that correlates with the utmost hardness. The trend observed is related to various aspects, namely the enhancement in mechanical properties, the strong nanofiller−matrix interfacial adhesion, the uniformly dispersed nanoparticles that decrease the free volume, and the elevated thermal conductivity of TiO_2 that reduces the temperature in the sliding contact.

A strong decrease is also found for the wear rate, and the nanocomposite with 7.5 wt% TiO_2 shows around 10-fold reduction in this property compared with that of AELO (Fig. 19.10B). This behavior could be ascribed to the improved stiffness combined with the rolling effect of hard inorganic nanoparticles such as TiO_2 that leads to the formation of a thin and uniform transfer film [48]. Such rolling mechanism was also described for epoxy/TiO_2 nanocomposites [49], and it was reported that TiO_2 not only behaved as a load carrier but also favored the bonding between the transfer film and the countersurface. Overall, the TiO_2 nanoparticles noticeably enhanced the mechanical and tribological properties of AELO.

4.6 Antibacterial Activity

Worldwide, millions of patients are affected annually by healthcare-associated infection (HCAI), which represents not only a public health risk but also an economic burden. HCAI can delay the length of hospital stays, lead to readmission after release, and augment costs to individuals and families. This has driven a strong interest in developing new strategies to reduce HCAIs, which are frequently related to invasive medical devices or surgical operations.

An increasing amount of these infections are caused by antibiotic-resistant pathogens, such as methicillin-resistant *S. aureus* (MRSA), *Clostridium difficile*, vancomycin-resistant enterococci (*VRE*), and carbapenem-resistant enterobacteriaceae (*CRE*). Viruses can also cause HCAIs, including HIV, hepatitis B, noroviruses, and coronaviruses. Sporadically, fungi, parasites, and prions are involved. Healthcare-associated infectious agents come from humans as well as from contaminated environmental objects and substances like air, food, water, table tops, ceilings, walls, doors, medical devices, and so forth. It is extremely imperative to prevent bacterial proliferation in hospital environments, principally in operation rooms, given that bacterial infections are the sixth foremost cause of death both in Europe and the United States.

To evaluate the suitability of AELO/TiO_2 nanocomposites as antimicrobial coatings in the health-care industry, their antibacterial activity was assessed versus gram-negative bacteria *E. coli* and gram-positive bacteria *S. aureus* that correspond to the 25% and 17% of the total hospital-acquired infections, respectively [41]. Before the experiments, the nanocomposites were sterilized in an autoclave and then immersed in a nutrient broth of $\sim 2.0 \times 10^6$ colony forming units per milliliter (CFU/mL). Subsequent to incubation at 37°C for 48 h, the number of viable microorganism colonies was counted manually with a pen and a click-counter, and the results were given as average CFU/sample. Experiments were performed both under 365 nm UV light and in dark conditions. The antibacterial activity was calculated as: $AA = \log(\text{viable cell count}_{control}/\text{viable cell count}_{composite})$, where a beaker containing bacteria and no sample was used as control. The results are shown in Fig. 19.11.

According to the ISO 22,196:2007 standard, effective antibacterial activity should be higher than 2 (marked as a dotted line on Fig. 19.11). AELO presents very small antimicrobial action versus *E. coli* and *S. aureus,* the result being the same with and without UV irradiation, in agreement with former works that reported the bactericidal activity of vegetable oils and found that it was influenced by their chain length and instauration degree [50]; it is believed that they can go through the cell wall and cause the break out of the cell contents.

Under both tested conditions, the antibacterial action improves with increasing TiO_2 content, attributed to the increase in the number of nanoparticles in contact with the bacterial membranes, hence more toxicity. This is consistent with previous studies that reported improved photocatalytic disinfection upon diminution in the bacterial cell−TiO_2 distance [51]. Further, the effect is influenced by the state of nanoparticle distribution within the matrix: the better the dispersion, the higher the bactericide action. This can explain that the nanocomposite with 7.5 wt% TiO_2 has similar activity to that with 5.0 wt%.

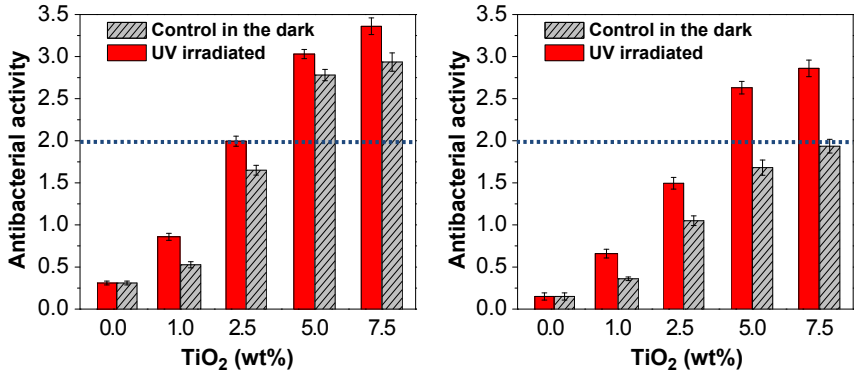

Figure 19.11 Antibacterial activity of acrylated epoxidized linseed oil (AELO)/titanium dioxide (TiO_2) nanocomposite coatings against human pathogen bacteria *Staphylococcus aureus* (left) and *Escherichia coli* (right).
Reprinted from A.M. Diez-Pascual, A.L. Diez-Vicente, Development of linseed oil−TiO_2 green nanocomposites as antimicrobial coatings, J. Mater. Chem. B 3 (2015) 4458−4471, copyright 2015, with permission from the Royal Society of Chemistry.

Under UV irradiation, *E. coli* proliferation is restrained when TiO_2 loading is $\geq$ 5.0 wt%, while *S. aureus* grow is hold back when the content is $\geq$ 2.5 wt% (Fig. 19.11), consistent with former works dealing with poly(lactic-*co*-glycolic acid) PLGA/TiO_2 nanocomposites that showed more efficient antibacterial activity against gram-positive bacteria [52]. As mentioned earlier, the efficiency of photocatalytic disinfection is related to the oxidative damage mostly provoked by ROS including O_2^-, HO_2, and HO radicals. OH radicals are supposed to be the major cause of the bactericidal effect [53], although some investigations attributed the antimicrobial action to the direct oxidation by "holes" from the valence band on the TiO_2 surface [54,55]. It has been proposed that initially ROS harm the outer membrane, and later damage the cytoplasmic membrane, implicated in the cellular respiration, hence the cell dies. The differences found between the two bacteria tested should be connected to structural and chemical differences of the cell surfaces. The cell wall of gram-positive bacteria comprises a thick, complex peptidoglycan sheath outside of the cytoplasmic membrane composed of peptidoglycan, teichuronic acids and lipoteichoic acids (Fig. 19.12A), while that of gram-negative microorganisms comprises an outer membrane connected to a thin single peptidoglycan film placed between the outer and inner membranes that contains lipopolysaccharides and lipoproteins and provides a permeability barrier of small hydrophilic molecules across the membrane (Fig. 19.12B). The outer membrane offers resistance to a number of substances, reducing the harm from ROS.

Experiments reveal that AELO/TiO_2 coatings have antibacterial activity in the dark, in agreement with preceding works that investigated the bactericidal action of this metal transition oxide in the absence of light [56]. Thus, just the nanocomposite with 7.5 wt% TiO_2 exerts a toxic effect on *E. coli* in the dark, while nanocomposites

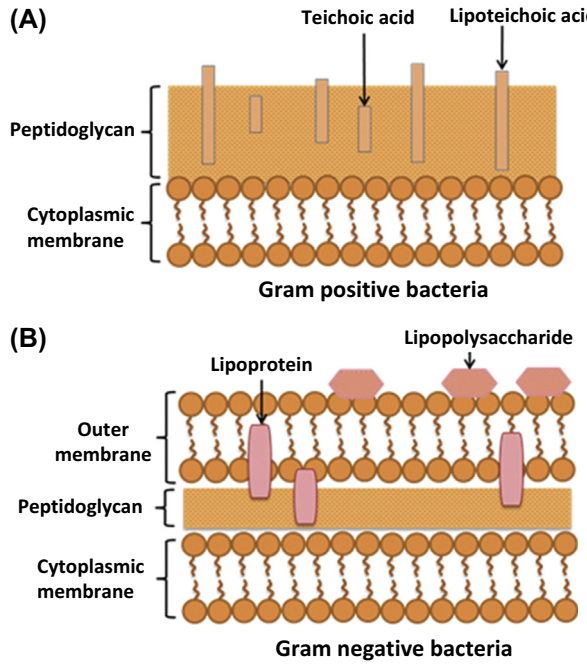

Figure 19.12 Structure of the cell wall of gram-positive (A) and gram-negative (B) bacteria.

with nanoparticle loadings ≥5.0 wt% show notable microbial action against *S. aureus*. These results disclose that apart from the photocatalytic process, other mechanisms should be responsible for the antibacterial action. Several of them have been reported [56], namely (1) nanoparticle adsorption onto the bacterial cell wall resulting in cellular damage; (2) redox reactions due to reduction of Ti(IV) to Ti(III) at the nanoparticle−baterial cell interface that provokes oxidative degradation of the cell membrane; (3) penetration of the nanoparticles in the cell and damage of the bacteria from the inside; (4) phagocytosis of the nanoparticles by the bacteria provoking the cell death. Besides, free radical formation at the bacteria surface in dark conditions has been proved [57]. Even though the accurate mechanism of TiO_2 antibacterial action is not clear up to date, the direct nanoparticle−bacteria contact appears to be decisive for efficient activity.

The antibacterial activity of AELO/TiO_2 was also evaluated by the agar-diffusion assay method, using third generation antibiotics, cefoperazone and cefixime, as positive controls versus *S. aureus* and *E. coli,* respectively. Zone diameter was measured after 24 h incubation under UV light at 37°C. Fig. 19.13 shows the images of the zone of inhibition for the different samples, and the results are summarized in Table 19.1. The larger the zone of inhibition, the more sensitive the bacteria is.

The agar-diffusion experiments confirm that AELO/TiO_2 nanocomposites have stronger antibacterial action versus gram-positive bacteria than against the gram-negative ones, and that the biocide effect increases with increasing TiO_2 content,

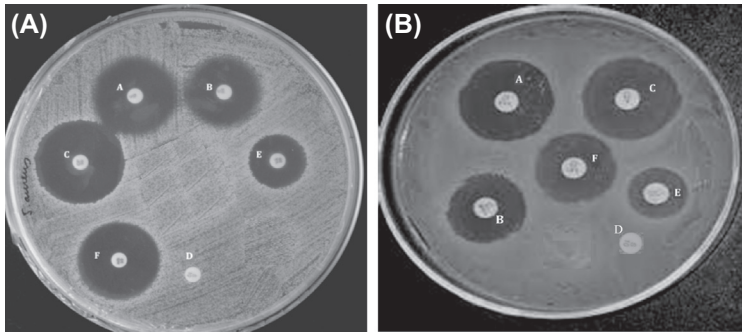

Figure 19.13 Zone of inhibition against *Staphylococcus aureus* (A) and *Escherichia coli* (B). The nomenclature of the samples is indicated in Table 19.1.

in agreement with data obtained from the colony-counting method. The highest diameters of growth inhibition zone are found for the nanocomposite with 7.5 wt% loading, close to those of the standard antibiotics, corroborating the susceptibility of the bacteria to this nanocomposite. The results of the agar-diffusion tests reveal the effectiveness of the developed coatings, particularly, that with the highest nanoparticle content, as antimicrobial agents. On the whole, AELO/TiO_2 nanocomposites show a great promise as antibacterial protections for public building applications.

Table 19.1 Antibacterial Activity of AELO/TiO_2 Nanocomposite Coatings Determined by the Agar-Diffusion Method

Sample	Well[a]	Zone of Inhibition Diameter (mm)	
		Escherichia coli	*Staphylococcus aureus*
AELO	D	0.0	0.0
AELO/TiO_2 (1.0 wt%)	E	9.5	11.4
AELO/TiO_2 (2.5 wt%)	B	13.9	16.0
AELO/TiO_2 (5.0 wt%)	F	15.9	18.9
AELO/TiO_2 (7.5 wt%)	A	18.6	20.3
Cefoperazone[c]	C	–	22.1
Cefixime[b]	C	20.3	–

[a]Wells shown in Fig. 19.13.
[b]Positive control against *E. coli*.
[c]Positive control against *S. aureus*.

5. Conclusions

In this chapter, the preparation and characterization of UV-cured AELO/TiO_2 antimicrobial nanocomposite coatings has been described, and their morphology, gas permeability, mechanical, thermal, tribological, and antibacterial properties have been discussed in detail. The nanoparticles improved the barrier properties, thermal stability, stiffness, strength, hardness, glass transition temperature, and wear resistance of the resin, and the best properties were found for the nanocomposite with 5.0 wt%. The coatings showed noticeable antibacterial activity both in the absence and in the presence of UV light, and the effect on gram-positive bacteria was thoroughly stronger than on gram-negative ones. These sustainable and environmentally friendly nanocomposite coatings show a great promise to prevent microorganism propagation on indoor public building materials, including hotels, libraries, museums, schools and universities, government edifices, railway and metro stations, and particularly, in the healthcare setting for sterilization of medical devices to diminish the hazard of getting infections. Examples are interior handrails in public buildings, patient room and intensive care units (ICU) entrances of hospitals and medical facilities, bed heads in hospitals, interior window frames of schools and historical buildings, entranceways of shopping centers, and so forth.

Acknowledgments

Dr. Ana Diez-Pascual wishes to acknowledge the Ministerio de Economía y Competitividad (MINECO) for a "Ramón y Cajal" Postdoctoral Fellowship cofinanced by the EU.

References

[1] G. Lligadas, J.C. Ronda, M. Galia, V. Cadiz, Renewable polymeric materials from vegetable oils: a perspective, Mater. Today 16 (2013) 337−343.
[2] J.-M. Raqueza, M. Deléglisea, M.-F. Lacrampea, P. Krawczaka, Thermosetting (bio)materials derived from renewable resources: a critical review, Prog. Polym. Sci. 35 (2010) 487−509.
[3] F. Gunstone, Fatty Acid & Lipid Chemistry, Blackie Academic & Professional, New York, 1996, pp. 1−252.
[4] R.R. Allen, M.V. Formo, R.G. Krishnamurthy, G.N. McDermott, F.A. Norris, N.O.V. Sonntag, Bailey's Industrial Oil and Fat Products, Wiley, New York, 1982.
[5] M.A. Mosiewicki, M.I.A. Aranguren, Short review on novel biocomposites based on plant oil precursors, Eur. Polym. J. 49 (2013) 1243−1256.
[6] M.A.R. Meier, J.O. Metzger, U.S. Schubert, Plant oil renewable resources as green alternatives in polymer science, Chem. Soc. Rev. 36 (2007) 1788−1802.
[7] R.P. Wool, Biobased Polymers and Composites, Elsevier Academic Press, Burlington (USA), 2005.

[8] M. Alam, D. Akram, E. Sharmin, F. Zafar, S. Ahmad, Vegetable oil based eco-friendly coating materials: a review article, Arab. J. Chem. 7 (2014) 469−479.
[9] A. Bayrak, M. Kiralan, A. Ipek, N. Arslan, B. Cosge, K.M. Khawar, Fatty acid compositions of linseed (*Linum usitatissimum* L.) genotypes of different origin cultivated in Turkey, Biotechnol. Biotechnol. Equip. 24 (2010) 1836−1842.
[10] F. Seniha-Güner, Y. Yagci, A. Tuncer-Erciyes, Polymers from triglyceride oils, Prog. Polym. Sci. 31 (2006) 633−670.
[11] G. Kaithwas, A. Mukerjee, P. Kumar, D.K. Majundar, *Linum usitatissimum* (linseed/flaxseed) fixed oil: antimicrobial activity and efficacy in bovine mastitis, Inflammopharm 19 (2011) 45−52.
[12] R. Wang, T.P. Schuman, Vegetable oil-derived epoxy monomers and polymer blends: a comparative study with review, Exp. Polym. Lett. 7 (2013) 272−292.
[13] L. Zhu, R.P. Wool, Nanoclay reinforced bio-based elastomers: synthesis and characterization, Polymer 47 (2006) 8106−8115.
[14] Y. Lu, R.C. Larock, Novel biobased nanocomposites from soybean oil and functionalized organoclay, Biomacromolecules 7 (2006) 2692−2700.
[15] A.M. Diez-Pascual, A.L. Diez-Vicente, Epoxidized soybean oil/ZnO biocomposites for soft tissue applications: preparation and characterization, ACS Appl. Mater. Int. 6 (2014) 17277−17288.
[16] A.M. Diez-Pascual, A.L. Diez-Vicente, Wound healing bionanocomposites based on castor oil polymeric films reinforced with chitosan-modified ZnO nanoparticles, Biomacromolecules 16 (2015) 2631−2644.
[17] K. Sunada, T. Watanabe, K. Hashimoto, Studies on photokilling of bacteria on TiO_2 thin film, Photobiol. Chem. 156 (2003) 227−233.
[18] L. Hochmannova, J. Vytrasova, Photocatalytic and antimicrobial effects of interior paints, Prog. Org. Coat. 67 (2010) 1−5.
[19] J.D. Cooley, W.C. Wong, C.A. Jumper, D.C. Straus, Correlation between the prevalence of certain fungi and sick building syndrome, Occup. Environ. Med. 55 (1998) 579−584.
[20] F. Fung, W.G. Hughson, Health effects of indoor fungal bioaerosols exposure, Appl. Occup. Environ. Hyg. 18 (2003) 535−544.
[21] H. Zhang, J. Huang, L. Yang, R. Chen, W. Zou, X. Lin, J. Qu, Preparation, characterization and properties of PLA/TiO_2 nanocomposites based on a novel vane extruder, RSC Adv. 5 (2015) 4639−4647.
[22] J.W. Rhim, H.M. Park, C.S. Ha, Bionanocomposites for food packaging applications, Prog. Polym. Sci. 38 (2013) 1629−1652.
[23] Z.F. Yin, L. Wu, H.G. Yang, Y.H. Su, Recent progress in biomedical applications of titanium dioxide, Phys. Chem. Chem. Phys. 15 (2013) 4844−4858.
[24] A. Kubacka, M. Fernandez-Garcia, M.L. Cerrada, M. Fernandez-Garcia, Titanium dioxide−polymer nanocompositeswith advanced properties, in: N. Cioffi, M. Rai (Eds.), Nano-Antimicrobials 4, Springer, Heidelberg, 2012, pp. 119−149.
[25] T. Kreetachat, J. Kruenate, K. Suwannahong, Preparation of TiO_2/bio-composite film by sol-gel method in VOCs photocatalytic degradation process, Appl. Mech. Mater. 390 (2013) 552−556.
[26] Y. Tang, Self-Cleaning Polyurethane and Polyester Coatings (Ph.D. thesis), University of Western Ontario, Electronic Thesis and Dissertation Repository, 2013. Paper 1098.
[27] M.R. Shaik, M. Alam, N.M. Alandis, Development of castor oil based poly(urethane-esteramide)/TiO_2 nanocomposites as anticorrosive and antimicrobial coatings, J. Nanomater. 2015 (2015) 745217.

[28] O. Carp, C.L. Huisman, A. Reller, Photoinduced reactivity of titanium dioxide, Prog. Solid State Chem. 32 (2004) 33−117.
[29] M.M. Byranvanda, A.N. Kharata, L. Fatholahib, Z.M. Beiranvand, A Review on synthesis of nano-TiO_2 via different methods, JNS 3 (2013) 1−9.
[30] M. Salari, S.M.M. Khoie, P. Marashi, M. Rezaee, Synthesis of TiO_2 nanoparticles via a novel mechanochemical method, J. Alloy Compd. 469 (2009) 386−390.
[31] A. Hassanjani-Roshana, S.M. Kazemzadeha, M.R. Vaezia, A. Shokuhfar, The effect of sonication power on the sonochemical synthesis of titania nanoparticles, J. Ceram. Process. Res. 12 (2011) 299−303.
[32] J. Liu, J. Xu, R. Che, H. Chen, M. Liu, Z. Liu, Hierarchical magnetic yolk−shell microspheres with mixed barium silicate and barium titanium oxide shells for microwave absorption enhancement, Chem. −A. Eur. J. 19 (2013) 6746−6752.
[33] A. Fujishima, K. Honda, Electrochemical photolysis of water at a semiconductor electrode, Nature 238 (1972) 37−38.
[34] H.M. Yadav, J.-S. Kim, S.H. Pawar, Developments in photocatalytic antibacterial activity of nano TiO_2: a review, Korean J. Chem. Eng. 33 (2016) 1989−1998.
[35] M.J. Hajipour, K.M. Fromm, A.A. Ashkarran, D. Jimenez de Aberasturi, I. Ruiz de Larramendi, T. Rojo, V. Serpooshan, W.J. Parak, M. Mahmoudi, Antibacterial properties of nanoparticles, Trends Biotechnol. 30 (2012) 499−511.
[36] K. Sunada, T. Watanabe, K. Hashimoto, Bactericidal activity of copper-deposited TiO_2 thin film under weak UV light illumination, Environ. Sci. Technol. 37 (2003) 4785−4789.
[37] G. Gogniat, M. Thyssen, M. Denis, C. Pulgarin, S. Dukan, The bactericidal effect of TiO2 photocatalysis involves adsorption onto catalyst and the loss of membrane integrity, FEMS Microbiol. Lett. 258 (2006) 18−24.
[38] H. Miyazaki, T. Hyodo, Y. Shimizu, M. Egashira, Hydrogen-sensing properties of anodically oxidized TiO_2 film sensors: effects of preparation and pretreatment conditions, Sens. Actuators, B 108 (2005) 467−472.
[39] J.H. Park, S. Kim, A.J. Bard, Novel carbon-doped TiO_2 nanotube arrays with high aspect ratios for efficient solar water splitting, Nano Lett. 6 (2006) 24−28.
[40] X. Chen, S.S. Mao, Titanium dioxide nanomaterials: synthesis, properties, modifications, and applications, Chem. Rev. 107 (2007) 2891−2959.
[41] A.M. Diez-Pascual, A.L. Diez-Vicente, Development of linseed oil−TiO_2 green nanocomposites as antimicrobial coatings, J. Mater. Chem. B 3 (2015) 4458−4471.
[42] D.W. Van Krevelen, Some basic aspects of flame resistance of polymeric materials, Polymer 16 (1975) 615−620.
[43] M.A. Sithique, M. Alagar, Preparation and properties of bio-based. nanocomposites from epoxidized soy bean oil and layered silicate, Malays. Polym. J. 5 (2010) 151−161.
[44] T.S. Radoman, J.V. Džunuzović, K.B. Jeremić, B.N. Grgur, D.S. Miličević, I.G. Popović, E.S. Džunuzović, Improvement of epoxy resin properties by incorporation of TiO_2 nanoparticles surface modified with gallic acid esters, Mater. Des. 62 (2014) 158−167.
[45] A.M. Diez-Pascual, M.A. Gómez-Fatou, F. Ania, A. Flores, Nanoindentation in polymer nanocomposites, Prog. Mater. Sci. 67 (2015) 1−94.
[46] H. Krenchel, Fibre Reinforcement, Akademisk Forlag, Copenhagen, 1964.
[47] V. Mittal, Polymer Nanocomposite Coatings, CRC press-Taylor & Francis, Florida, 2014, p. 117.
[48] K. Friedrich, A.K. Schlarb, Tribology of polymeric nanocomposites, in: J.B. Briscoe (Ed.), Tribology and Interface Engineering Series 55, Elsevier, Oxford, 2008.
[49] L. Chang, Z. Zhang, Tribological properties of epoxy nanocomposites-part II-a combinative effect of short carbon fibre with nano-TiO_2, Wear 260 (2006) 869−878.

[50] E. Medina, A. de Castro, C. Romero, M. Brenes, Comparison of the concentrations of phenolic compounds in olive oils and other plant oils: correlation with antimicrobial activity, J. Agric. Food Chem. 12 (2006) 4954−4961.
[51] S. Burt, Essential oils: their antibacterial properties and potential applications in foods−a review, Int. J. Food Microbiol. 94 (2004) 223−253.
[52] D. Gumy, C. Morais, P. Bowen, C. Pulgarin, S. Giraldo, R. Hajdu, J. Kiwi, Catalytic activity of commercial of TiO_2 powders for the abatement of the bacteria (*E. coli*) under solar simulated light: influence of the isoelectric point, Appl. Catal. B Environ. 63 (2006) 76−84.
[53] J.Y. Wu, C.W. Li, C.H. Tsai, C.W. Chou, D.R. Chen, G.J. Wang, Synthesis of antibacterial TiO_2/PLGA composite biofilms, Nanomed. Nanotechnol. 10 (2014) 1097−1107.
[54] Y. Kikuchi, K. Sunada, T. Iyoda, K. Hashimoto, A. Fujishima, Photocatalytic bactericidal effect of TiO_2 thin films: dynamic view of the active oxygen species responsible for the effect, J. Photochem. Photobiol. Chem. 106 (1997) 51−56.
[55] V. Nadtochenko, N. Denisov, O. Sarkisov, D. Gumy, C. Pulgarin, J. Kiwi, Laser kinetic spectroscopy of the interfacial charge transfer between membrane cell walls of *E. coli* and TiO_2, J. Photochem. Photobiol. Chem. 181 (2006) 401−407.
[56] S. Dalai, S. Pakrashi, S. Chakravarty, S. Hussain, N. Chandrasekaran, A. Mukherjee, Studies on interfacial interactions of TiO_2 nanoparticles with bacterial cells under light and dark conditions, Bull. Mater. Sci. 37 (2014) 371−381.
[57] L.K. Adams, D.Y. Lyon, P.J. Alvarez, Comparative eco-toxicity of nanoscale TiO_2, SiO_2, and ZnO water suspensions, Water Res. 40 (2006) 3527−3532.